JAAS

Accepted Manuscript

This is an *Accepted Manuscript*, which has been through the Royal Society of Chemistry peer review process and has been accepted for publication.

Accepted Manuscripts are published online shortly after acceptance, before technical editing, formatting and proof reading. Using this free service, authors can make their results available to the community, in citable form, before we publish the edited article. We will replace this *Accepted Manuscript* with the edited and formatted *Advance Article* as soon as it is available.

You can find more information about *Accepted Manuscripts* in the **Information for Authors**.

Journal Name

ARTICLE TYPE

Strontium speciation in archaeological otoliths

Phil K. Cook,[*a,b‡] Elise Dufour,[c] Marie-Angélique Languille,[a§] Cristian Mocuta,[b] Solenn Réguer,[b] and Loïc Bertrand[*a,b¶]

Fish otoliths ("ear stones") are major environmental indicators used in ecology and fisheries sciences. Otoliths consist of a biomineral material containing an organically-templated mineral calcium carbonate, normally aragonite, in which strontium is incorporated at minor to trace levels depending on water chemistry and individual physiology. Sr content and fluctuations inform on the life histories of ancient specimens and provide data for palaeoenvironmental reconstructions. Identifying the impact of *post-mortem* alteration is a critical question to assure the reliability of such work. A central parameter for the reliability of Sr content as a palaeoenvironmental proxy is whether the mode of incorporation can be considered as stable and homogenous at the microscale in otoliths over thousands of years. In addition, it is important to know whether a different kind of speciation of Sr is observed, especially at the outer surface of the sample in contact with the soil and local environment. Here, a novel combination of synchrotron microscale point analyses and raster-scanning X-ray absorption spectroscopy is implemented and used for the first time to study otolith at different length scales, spanning from millimetres down to micrometres. Strontium is found in substitution for calcium in aragonite in all our analyses of five Holocene otoliths and their three modern counterparts; the first set of samples from the Peruvian coast, up to 11 000 years old, are studied for their potential as palaeoenvironmental proxies. The chemical environment of strontium in otoliths is independent of content of this element, location in the otolith, species, and archaeological age. This is shown with a high lateral resolution (about 10 μm) over wide fields of view, as a way to consolidate macro-scale approaches. To our best knowledge, this work is the first report of the chemical environment of strontium in ancient otoliths. Our work opens the way to new approaches to validate palaeoenvironmental studies of biocarbonate palaeoproxies.

[a] IPANEMA, CNRS, ministère de la Culture et de la Communication, USR3461, Université Paris-Saclay, F-91192 Gif-sur-Yvette, France.

[b] Synchrotron SOLEIL, F-91192 Gif-sur-Yvette, France.

[c] Archéozoologie, archéobotanique: Sociétés, pratiques et environnements (UMR 7209), Sorbonne Universités, Muséum national d'Histoire naturelle, CNRS, CP55, 55 rue Buffon, F-75005 Paris, France

† Electronic Supplementary Information (ESI) available: Additional figures and tables. See DOI: 10.1039/b000000x/

‡ Current address: ESRF – The European Synchrotron, CS 40220, 71 avenue des Martyrs, F-38043 Grenoble, France. E-mail: philip.cook@esrf.fr

§ Current address: Centre de recherche sur la conservation (CRC, USR 3224), Sorbonne Universités, Muséum national d'Histoire naturelle, Ministère de la Culture et de la Communication, CNRS ; CP21, 36 rue Geoffroy-Saint-Hilaire, F-75005 Paris, France.

¶ E-mail: loic.bertrand@synchrotron-soleil.fr

1 Introduction

Teleost otoliths ("ear stones") are biomineral accretions, three pairs of which are found in the inner ear of fish.[1] An organic template comprising 1–10 %wt of the otolith guides the deposition of the mineral phase.[2] The mineral phase, comprising the remaining 90–99 %wt is composed of calcium carbonate ($CaCO_3$) with some minor and trace elements. The $CaCO_3$ in living fish otoliths is normally in the aragonite polymorph.[3] Calcite and vaterite can be found in some species for one of the less-developed otolith pairs[4] or in case of pathologies.[5–7] Otoliths grow in increments from the center to the core in periodic growth marks reported at the macro or micro-scale.[8] Increments can be assumed to be at the heart of otolith biomineralisation by analogy with the morphology and role of nanogranules in molluscs.[9] Over the past few decades, geochemical analyses — determination of elemental and isotopic compositions — of fish otoliths have pro-

vided a wealth of information about the biology of fish and the environments frequented over the life of an individual. During accretional growth the otolith aragonite and the organic matter can incorporate trace and minor elements. At least 27 such elements have been reported, of which Na, K, P, and Sr are typically found in the highest concentrations. [10] Sr concentration (typically up to $51 \mu mol \cdot g^{-1}$ (equivalent to $4.5 mg \cdot g^{-1}$), exceptionally up to $137 \mu mol \cdot g^{-1}$ ($12 mg \cdot g^{-1}$) [10,11]; usually normalised to Ca content) is the most widely used environmental tracer in fish and fisheries sciences, while physiological effects and a possible impact of diet can also be observed. [12] Incorporation of Sr into fish otoliths is dependent primarily on water chemistry, and on the ambient temperature [13,14] under physiological control.

The elemental and stable isotopic signals from ancient otoliths are being applied more frequently for various types of studies [10,15]: biological and environmental archives for the study of past fish migration or metabolism [16,17], palaeoenvironmental and palaeoclimatic conditions from the Jurassic to the Holocene [18–22], and fishing practices of past human populations. [22–25] The reliability and permanence of the geochemical information encoded within ancient otoliths is critical to their use as information archives. Diagenesis might hamper such reconstructions from ancient samples, and the level of this alteration in the otoliths has to be estimated. [21,26] When Sr content is used as a palaeoenvironmental proxy, its local mode of incorporation and stability within the organic fraction of otoliths and/or in the aragonite biomineral are likely of crucial influence on its long-term behaviour, and therefore its reliability. [27] No previous work reports on elemental speciation in ancient fish otoliths. Working at the microscale is necessary as alteration could occur not only in the whole otolith, but also in localised zones. [21,26] The outer zones of the otolith are expected to be more susceptible to alteration as a result of their direct contact with the surrounding environment [28], including fluids such as those from the decaying animal, although there is evidence for some sort of pore network throughout otoliths, making the entire object subject to potential alteration. [29]

Central questions are therefore whether: (a) Sr speciation in otolith samples with no present evidence of alternate carbonate polymorph can be considered as homogenous and stable at micrometre scales, (b) sample areas with significant elemental or isotopic excursions could show a specific mode of incorporation of Sr, (c) outer surfaces of samples, possibly containing exogenous ions, could show a distinct speciation of Sr. Information on the chemical environment of Sr can be collected through X-ray absorption spectroscopy. [30–32] However, past works on corals illustrate the difficulty of distinguishing between minerals such as strontianite ($SrCO_3$) and Sr-containing aragonite (noted below 'Sr:aragonite') due to their isostructural character. [33,34]

This work is, to our best knowledge, the first determination of the chemical environment of a major environmental proxy, strontium, in ancient otolith specimens. An approach was developed using synchrotron X-ray absorption spectroscopies (XAS) at distinct successive length scales (from mm down to μm). A focused X-ray beam permits analysis of a selected micrometer-scale sample volume. Synchrotron-based XAS is shown to be capable of clearly elucidating Sr speciation, in particular by comparing the imaginary component of the Fourier-transform signals. The lateral resolution (resolution in the plane of the sample surface) afforded was used to select limited illumination areas with different Sr concentrations for analysis, such as the outer edge or a significant excursion from average Sr concentration. A millimetric area on an archaeological sample was examined to confirm the homogeneity of Sr speciation, over a span in length scales of several to several hundred micrometres. The Sr chemical environment was universally confirmed to be Sr in aragonite, with no evidence for the presence of other mineral phases on the scale of these analyses, on five archaeological and three modern otoliths from the Pacific coast of South America exhibiting a wide range of Sr concentrations. We discuss the methodological and diagenetic implications of these results.

2 Materials and methods

2.1 Archaeological and modern fish otoliths

Archaeological otoliths from excavations in northern Peru at Pampa de los fósiles, Huaca Prieta, and Bayovar-1, were chosen because of their potential for palaeoclimatic information. [35–37] They form part of a larger study of palaeoenvironmental conditions and past human occupation in a region that lacks palaeoclimatic proxies. [35] Otolith specimens of five archaeological and three modern fishes from the tropical Pacific coast of South America have been examined (Tab. 1). The specimens all come from coastal marine species of Sciaenidae (*Micropogonias* sp., *Micropogonias altipinnis*, *Micropogonias manni*) and Ariidae (*Galeichthys peruvianus*, *Cathorops* sp.). In these two families the most-developed otolith pair (of sagittae, lapilli, and asterisci) is different: Sciaenidae present more developed sagittae while Ariidae present more developed lapilli. [39] Sections were prepared from otoliths embedded in resin. Details can be found in *Supplementary Information* SI.1. The section of otolith QCD could be removed from the glass slide after polishing and analysed without other support, while it was not attempted for the other sections owing to their apparent fragility.

Preliminary examination

After preparation, the otolith sections were examined for obvious alteration using light microscopy (LM), scanning electron microscopy (SEM), Fourier transform infrared (FT-IR, not shown here) spectroscopy, and X-ray diffraction (XRD, not shown here). FT-IR spectra were collected in reflection mode with a spot size of $350 \mu m$ (Paleoproxus, IRD, Bondy). XRD data were collected from subsamples of otoliths with Cu Kα radiation. Local crystal ordering was also studied on some samples using synchrotron XRD. LM and SEM examination of the samples (Figs. S1-S3) indicate that none of them exhibit significant microstructural alteration. Subsamples of HP-11, HP-12, and GP-292 were confirmed to be aragonite by XRD. Samples QCD, Bayovar-1C, 111, and BH17 were examined by FT-IR spectroscopy at 3–11 points each, all of which were identified as aragonitic.

Table 1 Information on the µXAS analysis points on the five archaeological and three modern otolith samples. Geological sample ages in years before present (BP) correspond to the age of the stratum in which an otolith was discovered. A µEXAFS spectrum was recorded at the analysis points marked with *. Letter annotations in the far right column correspond to points in Fig. 1

Name	Species	Sample age	Origin	Section thickness (µm)	[Sr] range (µmol·g⁻¹)	[Sr] at analysis points (µmol·g⁻¹)
QCD	*Micropogonias* sp.	Preceramic (Paíjan) 11 000–8000 BP [38]	Pampa de los fósiles, Cupisnique Desert, Peru	710	27–51	36.6 (A), 35.0 (B), 39.7 (C), 36.2* (D), 27.2 (E), 50.7 (F), 40.4 (G)
HP-11	*Galeichthys peruvianus*	Preceramic 4140±40 BP	Huaca Prieta, Chicama Valley, Peru	150	21–185	42.1 (A), 48.5 (B), 62.5 (C), 58.5 (D), 53.1 (E)
HP-12	*Galeichthys peruvianus*	Preceramic 6641±49 BP [36]	Huaca Prieta, Chicama Valley, Peru	130	21–101	60.0 (A), 79.5 (B), 93.3* (C), 90.5 (D), 93.9 (E), 74.9 (F), 64.5 (G), 49.0 (H)
Bayovar-1C	*Micropogonias* sp.	Early Intermediate Period (200 BC–600 AD) – beginning Middle Horizon (600–1000 AD) [37]	Bayovar-1, Sechura Desert, Peru	490	17–50	18.4, 48.7*
BH17	*Cathorops* sp.	Preceramic (Paíjan) 11 000–8000 BP [38]	Pampa de los fósiles, Cupisnique Desert, Peru	260	17–60	54.1*
424	*Micropogonias manni*	17/11/2005	Budi, Chile	290	14–22	14.9, 15.7, 16.8, 21.5, 22.2*
111	*Micropogonias altipinnis*	14/06/2000	Puerto Lopez, Ecuador	460	7–12	7.1, 12.2*
GP-292	*Galeichthys peruvianus*	26/03/2012	Chorillos, Peru	160	15–52	29.1, 51.1*

2.2 Reference materials

Three reference compounds were selected for comparison to assess the chemical environment of Sr in our samples: natural aragonite ($CaCO_3$, Alfa Aesar, batch I15T027), natural calcite ($CaCO_3$, Alfa Aesar, batch C08S004), and synthetic strontianite ($SrCO_3$, 99.994% pure, Alfa Aesar, batch 23669). All references were prepared neat, except for strontianite, which was diluted with synthetic calcite (VWR, lot DBJ 150004) and with 6.8 %wt microcrystalline cellulose (Merck, batch K36832831 733) during grinding to an equivalent 0.4 %wt in Sr in order to limit autoabsorption of fluoresced X-rays. Each material was prepared by grinding into a fine, homogeneous powder in a clean agate mortar and pestle for 5 minutes, then pressed into a pellet in a 13 mm die. The fundamental parameters for Sr quantification were experimentally determined from processing the mean spectrum from a 1×1 mm² grid of 10×10 points on a pellet of fish otolith Certified Reference Material no. 22 (CRM22, National Institute for Environmental Studies, Tokyo, Japan). [40]

2.3 Synchrotron methods

Synchrotron X-ray fluorescence and micro-X-ray absorption spectroscopy measurements using a microscopic beam (respectively denominated µXRF and µXAS) were implemented at the DiffAbs beamline of the SOLEIL synchrotron. [41] The beam was focussed using achromatic Kirkpatrick-Baez mirrors [42] to a spot size of 6.0×11 µm² full width at half maximum (FWHM, V×H) with an on-sample flux of *ca.* 3×10^9 ph/s. The incident photon flux (I_0) was recorded by a 10 µm-thick thin film Si diode (Hamamatsu

Photonics) in transmission. The samples were mounted in-air on a goniometer at 45° to both the incident beam and detector, with the growth axis parallel to the 6.0 µm axis of the beam to maximise the lateral resolution across isochronous increments. This resulted in an effective spot size on the sample of 6.0×16 µm². Sample fluorescence was recorded using a Vortex-EM monoelement silicon drift fluorescence detector (50 mm² active area, Hitachi) with a Digital Pulse Processor (Hitachi). The detector was placed in the same horizontal plane at 90° from the beam to minimise X-ray scattering contribution. The sample–detector distance was optimised for each sample to maximise the detected signal while remaining within the detector's range of linear response.

2.3.1 Synchrotron micro-X-ray fluorescence

Elemental µXRF maps were collected to identify areas of interest for X-ray absorption measurements, and estimate Sr and Ca concentrations and distribution. Maps were collected using an incident beam energy of 16 200–17 200 eV. Quantification was carried out using PyMca [43] and the methodology described by Cook *et al.* [27] XRF maps additional to those in Fig. 1 are present in the latter article. After determining the basic fitting parameters, the photon flux was evaluated using the reference's certified Sr mass fraction. [40]

2.3.2 Synchrotron X-ray absorption spectroscopy

All XAS data were collected around the Sr K-edge at $E_0 \approx 16 104.5$ eV. X-ray absorption near edge spectroscopy (XANES) spectra on reference materials were recorded in transmission mode using a wide X-ray beam (on-sample spot size *ca.* 250×300 µm² FWHM, flux *ca.* 5×10^{12} photons/s) to limit the im-

pact of microscale heterogeneity of the standards. Ionisation chambers (N_2 gas, 200 V operating voltage) provided photon flux monitoring before and after the sample. Reference spectra were recorded with a count time of 3 s/point in three ranges: 15 902–16 030 eV in 2 eV steps, 16 032–16 132 eV in 1 eV steps, and 16 134–16 250 eV in 2 eV steps.

X-ray absorption spectroscopy measurements with a microscopic beam (μXAS) were performed with fluorescence yield detection using the same configuration and detector as for μXRF. The μXAS signal was calculated by numerically integrating a 600 eV wide window centered on the Sr Kα fluorescence peak. Total count rates up to *ca.* 130 and 115 kcps were measured on the white line and in the post-peak region, respectively, with the Sr Kα peak contributing *ca.* 51 and 36 kcps. The integrated signal was corrected for detector deadtime and normalised to I_0 as measured by the thin film diode. Microscale XANES (μXANES) spectra of otolith samples were recorded with a count time of 4 s/point in the 16 023–16 083 eV energy range in 2 eV steps, 16 084–16 134 eV in 1 eV steps, and 16 135–16 373 eV in 2 eV steps. Microscale extended X-ray absorption fine structure (μEXAFS) spectra were recorded with a count time of 8 s/point for 16 023–16 083 eV in 2 eV energy steps, 16 084–16 224 eV in 1 eV steps, and 16 225–16 773 eV in 2 eV steps (Fig. 2 and 3). All spectra were processed using the iXAFS suite version 2.2 including ATHENA (data extraction), ARTEMIS (fitting of spectra), and IFEFFIT (ab initio multiple scattering calculations).[44] Details on the extraction and treatment of EXAFS spectra can be found in *Supplementary Information* SI.2.

E_0 was determined using the procedure discussed in *Supplementary Information* SI.2 due to a complex edge with multiple inflection points. In four spectra — archaeological specimens Bayovar-1C ([Sr] = 48.7 μmol·g⁻¹; Fig. 3b) and HP-12 ([Sr] = 90.5 and 93.3 μmol·g⁻¹; *Supplementary Information* Fig. S5), and modern specimen 111 ([Sr] = 12.2 μmol·g⁻¹; Fig. 3b) — we observed variations in the maximum intensity and position of the white line. This is attributed to a flattening of the peak when recording with a high count rate where the detector was operating at the limits of the linear range. The otolith aragonite is also strongly textured with the *c* axis of the crystals showing a preferential orientation along growth axis, which could lead to noticeable change in the white line intensity with respect to the beam polarisation.

μXANES mapping was performed using a reduced dataset on the section of QCD. Four diagnostic energies were selected to provide significant discrimination between aragonite and strontianite based on the μXANES spectra of reference inorganic aragonite and strontianite (as identified in Fig. 3a: 16 149, 16 170, 16 185 and 16 201 eV). A μXRF map was recorded at each of these four energies.[45] A crack in the otolith was observed and was excluded from the analysis zone, leaving final map dimensions of $570 \times 450\,\mu m^2$ (V×H). Assuming that the chemical environment of strontium is a mixture of aragonite and strontianite, fraction aragonitic and fraction strontianitic environment were deduced using procedures written under the 'R' statistical environment[46] on a per-pixel basis.
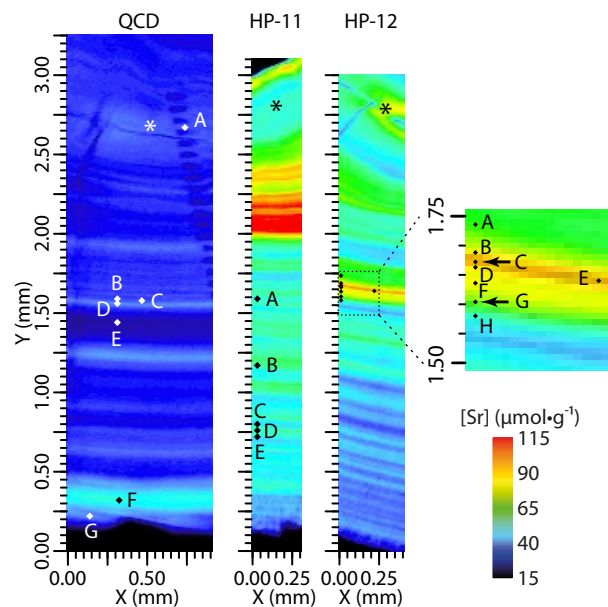
Fig. 1 μXRF maps of strontium distribution in archaeological samples of *Micropogonias* sp. (QCD, Pampa de los fósiles, Peru) and *G. peruvianus* (HP-11 and HP-12, Huaca Prieta, Peru). ◆ marks points analysed by μXANES, except QCD (D) and HP-11 (C) which are μEXAFS analysis points. Otolith cores are marked with asterisks.

3 Results

The methodological approach, applied to both ancient and modern otoliths, used in the determination and speciation Sr involves a three step process: (1) single point μEXAFS analysis provides a detailed overview of Sr speciation at specific locations on the sample, (2) collection of series of μXANES allows comparison of Sr chemical environment intra- and inter-samples, and (3) μXANES mapping allows checking and validating Sr speciation across large areas of samples.

Spots where XAS was performed were identified from XRF maps of archaeological otolith sections. Sr elemental maps show both intra-individual and interspecific variability in Sr content (Fig. 1). The total range of Sr concentration variation for the eight specimens is 7–180 μmol·g⁻¹. Note that the maximum concentration in Sr further extends the upper range reported for this element.[27]

3.1 EXAFS characterisation of strontium in archaeological otoliths

Point μEXAFS at strontium K-edge spectra were recorded on 7 otolith sections (Tab. 1) to precisely compare and model X-ray absorption features. A spectrum from QCD is presented in Fig. 2 and 3 as a general representative of that from the archaeological otolith samples compared to the inorganic references. An asymmetric peak just above 2 Å is present in the Fourier transform (FT) magnitude of all three spectra. As discrimination between Sr:aragonite and strontianite is not straightforward, both magnitude and imaginary parts of the FT of μEXAFS spectra were compared. Qualitatively, the FT of QCD closely resembles that of aragonite (Fig. 2). Fitting of the EXAFS was performed (Tab. S2)
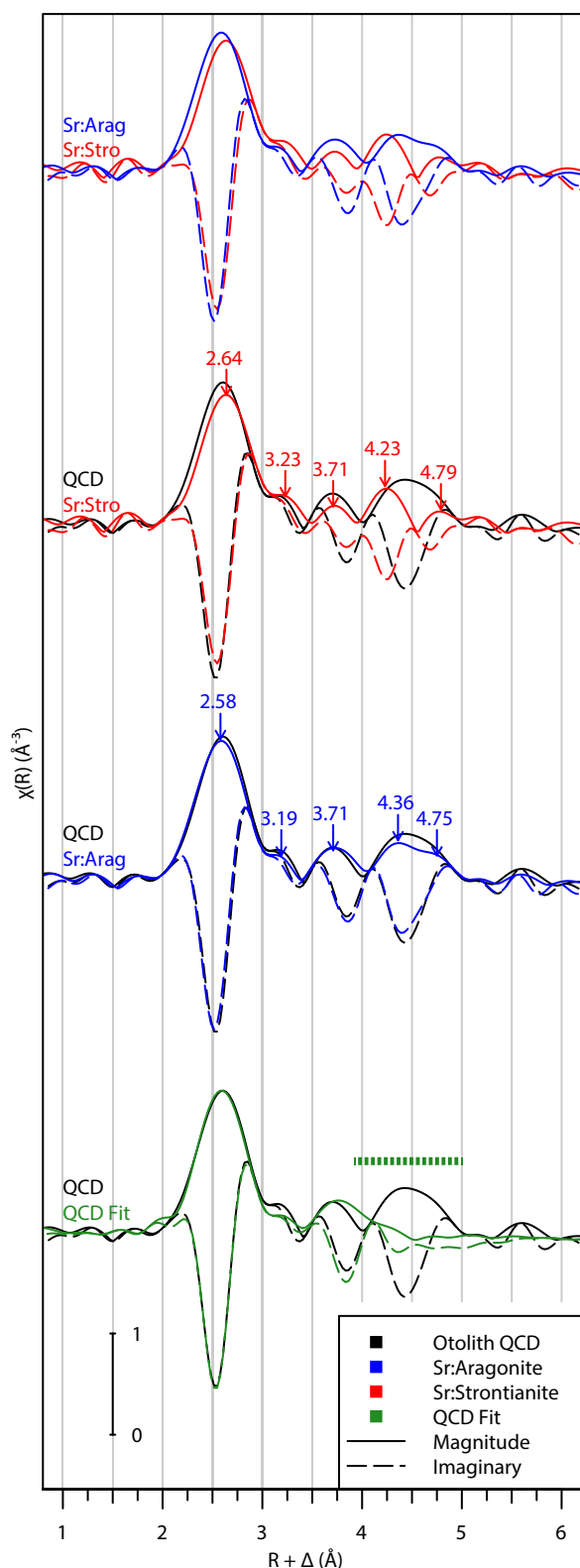
Fig. 2 Magnitude and imaginary part of the phase-corrected Fourier transforms of μEXAFS spectra at Sr K-edge (beam size $6.0 \times 16 \, \mu m^2$ FWHM) of archaeological *Micropogonias* sp. otolith QCD (Pampa de los fósiles, Peru, [Sr]=$36.2 \, \mu mol \cdot g^{-1}$) compared to those of inorganic reference materials aragonite and strontianite, and the fitted spectrum. The FT of QCD is typical for all otolith samples. Features in the section of the bottom spectrum designated by a bar were not fitted (see text for explanation).

for both references and otolith samples. Reference natural aragonite and synthetic strontianite exhibit Sr–M (M: metal, *i.e.* Ca or Sr, resp.) lengths of 3.980 and 4.155 Å, respectively. All otoliths exhibit Sr–M lengths in the range of 3.965–3.988 Å, which corresponds closely to that identified in the aragonite reference. These distances are also coherent with those reported in previous works on modern carbonate biominerals and strontianite chemistry.[31,32,34,47] Fits of the distinct EXAFS spectra resulted in good agreement to the experimental data for the first O, C, and Ca shells up to 4.0 Å in aragonite and QCD, and to 4.5 Å in strontianite. Inclusion of additional O shells and multiple scattering paths was not attempted, which explains the deviation between the data and fit in the 4–5 Å range, also observed by other authors for identical reasons.[47]

3.2 XANES characterisation of strontium in archaeological otoliths

Macro-XANES spectra at Sr K-edge on the archaeological otolith sample QCD provide spectra with a high signal-to-noise ratio while averaging possible microscopic fluctuations (Fig. 3a). The spectrum of QCD exhibits the following features, where energies are referred to as a shift relative to E_0 (*i.e.* $E_0 + n$ eV): (i) no evident pre-edge features; (ii) $E_0 = 16\,104.4$ eV; (iii) a white line with several inflection points observable in the spectrum derivative (Fig. S4); (iv) a white line maximum at +7.3 eV (16 112 eV); (v) a low intensity absorption feature at *ca.* +20.8 eV; (vi) oscillations with a first significant maximum at +43.4 eV preceded by a shoulder at *ca.* +30 eV; (vii) a shoulder at +65 eV; and (viii) a third somewhat sharp maximum at +94.1 eV. All these features are accurately shared by the inorganic aragonite reference. The spectrum of inorganic aragonite also exhibits some similarity to that of the strontianite reference, with some differences: the low-intensity feature at +20.8 eV (iv) and the shoulder at *ca.* +30 eV (vi) are absent, and the oscillation at +94.1 eV is very broad. To permit analysis of a wide variety of zones and check for intra-sample homogeneity, between one and 8 μXANES spectra at Sr K-edge per sample were collected for all samples and compared to the macro-XANES spectra (Tab. 1). The characteristic features, including the small oscillation at +20.8 eV, oscillation and shoulder at +43.4 and +65 eV, and the oscillation at +94.1 eV are consistent for all otoliths (Fig. 3b). The relative intensity and sharpness of the white line does vary slightly in some areas, as mentioned previously. Apart from the white line, spectra all show superimposable features (*Supplementary Information* Fig. S5). No variation is observed in the position of E_0 nor any of the characteristic oscillations. Point analyses cover an overall Sr concentration range of 27–95 $\mu mol \cdot g^{-1}$.

3.3 μXANES mapping of strontium chemical environment in the archaeological otolith QCD

To assess the representativeness of point X-ray absorption measurements over large 'spatial dynamics',[48] μXANES mapping was carried out using four energies selected to correspond to characteristic features observed in the XANES spectra at Sr K-edge of the aragonite and strontianite standards (marked by the dashed
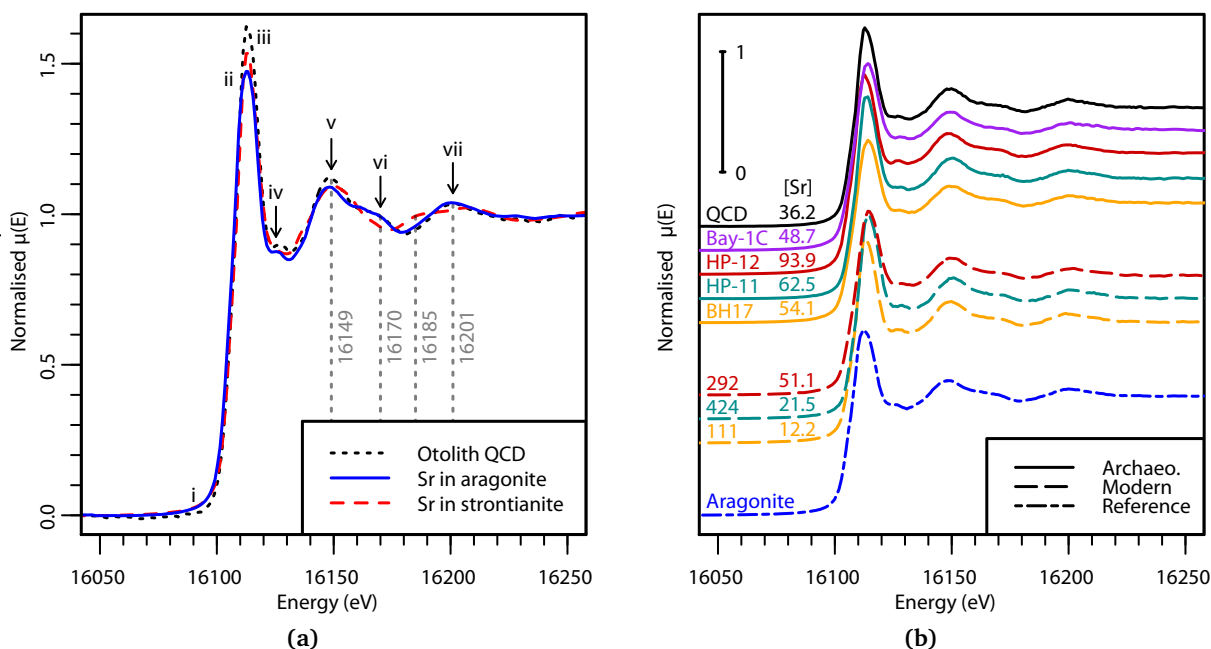
Fig. 3 (a) XANES spectrum at Sr K-edge of archaeological *Micropogonias* sp. sample QCD (Pampa de los fósiles, Peru) compared to inorganic aragonite and strontianite references. Spectral features (i–vii) are described in the text. Vertical lines mark selected characteristic energies used for μXANES mapping in Fig. 4. (b) Comparison of XANES spectra at Sr K-edge μof 8 otoliths from four species at three archaeological sites and three modern locations with inorganic aragonite. Spectra have been shifted vertically. The Sr concentration at the point of analysis in $\mu mol \cdot g^{-1}$ is indicated next to each sample name.

lines in Fig. 3a). μXRF maps were collected on archaeological sample QCD at these energies across areas up to $570 \times 500 \, \mu m^2$ (Fig. 4). The Ca concentration map (Fig. 4c) shows limited variation aside from an enhancement at the outer edge. The Sr concentration map (Fig. 4d) reveals a total range of 19–39 $\mu mol \cdot g^{-1}$ in the mapped zone, with a maximum value close to the edge. The map of aragonite fraction is shown in Fig. 4e. The map exhibits high homogeneity with a standard deviation (SD) of 7.2 % in a unimodal distribution across the full mapped area, centered on 91 % aragonite (Fig. 4f). The SD along the growth axis (7.5 %) – in the direction of Sr variations – is comparable to the SD within a growth increment (7.2 %), and the per-increment median covers a range of ±8 %. Profiles along the growth axis can be calculated from integration along isochronous increments (Fig. 4g). The maximum Sr concentration at the sample edge (Fig. 4g, "Max") corresponds to the maximum observed on the entire otolith, while the minimum ("Min") is only a local minimum with lower concentrations elsewhere along the growth axis (Fig. 1). Some substructure can be seen in the transition between high and low Sr areas ("SS"). Most interestingly, the fraction of aragonitic environment determined through the processing of multi-energy XANES maps shows no relation to variation in Sr content, nor distance to the sample edge.

4 Discussion

Ancient biominerals recovered in archaeological and paleontological contexts provide key evidence for reconstructing past human activity, and climatic or environmental conditions. The potential to use the geochemistry of ancient otoliths as information

archives has long been recognized and is now fostering significant development in archaeology. Recently, geochemical analyses have been used to reconstruct the ambient conditions experienced by fish to then gain insight into the functioning of aquatic environments themselves as well as fish movements and adaptation to these environments.[21,22,49] Further, knowledge on fish palaeoecology and palaeoenvironment can be used for reconstruction of fishing practices (exploited aquatic habitats, season of fishing) and site occupancy by past human populations.[22–24,35,36,50]

Interpreting the geochemistry of ancient biominerals is, however, challenging, requiring an understanding of the physical and biological processes of incorporation (element partitioning or isotopic fractionation) and interpretation of *post-mortem* changes linked to pre- and post-burial environment. If a biomineral proxy undergoes *post-mortem* alteration, this could lead to a significant impact on the reliability of the biogenic geochemical information encoded within. In this respect, otoliths have far less been studied than other biominerals such as bones[28,51–54], enamels[55,56], shells[57–59], or corals.[60,61] As a standard practice, altered otolith specimens are distinguished from unaltered ones by detection of microstructural alteration and/or change in the identity of calcium carbonate polymorph.[26] An intact microstructure is defined by the presence of growth marks typical of otoliths (daily and yearly increments),[23] long needle-like (prismatic) aragonite crystals,[26,62,63] and/or the absence of recrystallised or neoformed minerals.[7,17,18,26,62] Aragonite is metastable and will tend to transform to calcite over time.[59] The absence of calcite and vaterite is considered an indicator of geochemical preservation. Transformation to another crystal polymorph can be detected
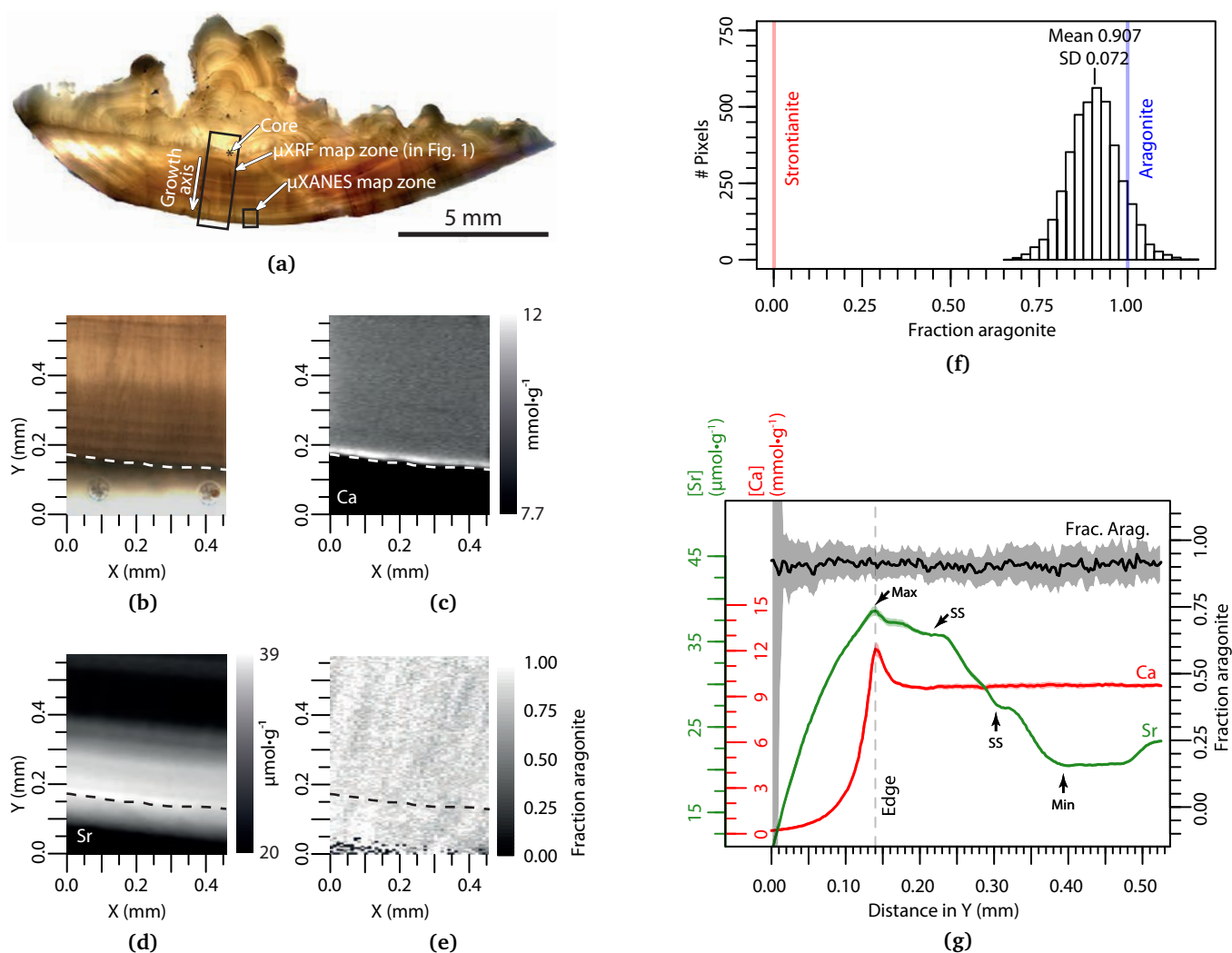
Fig. 4 Homogeneity of the speciation of strontium in a zone from the archaeological *Micropogonias* sp. otolith QCD section (Pampa de los fósiles, Peru). (a–b) Light microscopy images. (a) Image of sample with positions of analyses indicated. (b) Magnified image of the analysed zone corresponding approximately to 1.5 years' growth. The dashed line indicates the otolith edge. (c–g) Results from synchrotron speciation mapping. (c) Concentration map of Ca in $\mathrm{mmol \cdot g^{-1}}$. (d) Concentration map of Sr in $\mathrm{\mu mol \cdot g^{-1}}$. (e) Map of the estimated fraction of aragonite. (f) Histogram of aragonite fraction. The pixels outside of the otolith (black in map c) were excluded from the histogram. The values for pure strontianite and pure aragonite are marked with vertical lines. (g) Profiles along the growth axis integrated along isochronous increments for elemental concentrations of Ca and Sr, and aragonite fraction: median (solid line), ± 1 standard deviation (shaded areas). Arrows indicate features in the [Sr] curve discussed in the text.

by X-ray diffraction[7,18,26,63–65], vibrational spectroscopy[62], or cathodoluminescence.[7,62,65] The quality of preservation of the pristine geochemical signal measured in ancient otoliths can also be assessed through comparison to the otoliths of modern individuals of the same species or of a taxonomically close species which are expected to exhibit similar geochemical signatures.[26,27] Conversely, otoliths of taxa with different ecologies can be compared in order to reveal expected contrasts in different geochemical signatures.[26,63]

Although a limited number of works were dedicated to specific aspects of diagenesis in ancient otoliths,[26,27,62] no comprehensive study of speciation in ancient otoliths has been conducted so far. The present paper constitutes a first effort to determine the chemical environment of Sr in archaeological otoliths to decipher the long term behavior of this element. The ability to not only detect alteration, but to potentially designate particular areas as reliable or not, and correlate it to sample morphology and/or other characteristics would be highly useful to ensure the reliability and full exploitation of palaeo-environmental analyses. There is therefore a need to identify whether Sr is present in substitution to Ca in aragonite, as strontianite $SrCO_3$ domain, or in other mineralogical forms, in ancient otoliths.

Incorporation of secondary elements into carbonate biominerals can possibly be categorised into three main modes: (1) intra-crystalline incorporation (substitution for Ca, incorporation as interstitials) and/or adsorption onto crystal surfaces, (2) incorporation into the organic material, or (3) as discrete phases of a secondary mineral. In aragonite, Ca is coordinated to 9 oxygen ions while coordination number is 6 in calcite. Sr is assumed to substitute isomorphously for Ca owing to the similar charge and ionic radius of the two ions: 118 pm for Ca^{2+} and 131 pm for Sr^{2+} in 9-fold coordination (Tab. S1).[66–68] Sr (or any other element) adsorbed on the surface or incorporated into the organic material is expected to be less stable than in the crystal lattice.[69] Sr is not significantly leached out during handling or preparation (cleaning, sectioning, polishing, staining, and etching) of otoliths at the laboratory.[69–72] Indeed, this has generally been interpreted as Sr incorporation into the aragonite lattice[70,71] but has alternatively been interpreted as the presence of stable strontianite domains.[69] Areas exposed to specific *post-mortem* alteration mechanisms (e.g. surface) could lead to distinct modes of incorporation for Sr.

4.1 µXAS analyses ubiquitously indicate Sr in aragonite at micrometric scales

We examined the chemical environment of Sr at the microscale in 5 archaeological otoliths from the Holocene, and 3 modern counterparts. Our point X-ray absorption spectroscopy results globally indicate Sr in an aragonitic environment within the limits of detection:

(1) Distinction from calcite or vaterite environments is relatively straightforward as both crystallize in a distinct mineralogical form (Tab. S1). Both polymorphs therefore exhibit a distinctly different XANES spectrum at Sr K-edge from aragonite, with in particular a double peak at the white line.[31,73] Such a feature was never observed on spectra of the present work. We can therefore rule out the presence of calcite or vaterite as a significant environment for Sr at *any sample point* studied. This observation fulfills one of the common conditions for preservation of the geochemical signal, absence of $CaCO_3$ polymorphs other than aragonite, while extending it to a micrometer scale.

(2) Distinction of aragonite from strontianite is a more challenging task.[33,34] In the EXAFS Fourier transform (FT) magnitude of the strontianite reference, the Sr–Sr signal at 3.95 Å appears slightly removed from the inorganic aragonite Sr–Ca signal at *ca.* 3.90 Å, which is shared by all otoliths (Fig. 2). A slight difference in FT magnitude between strontianite and aragonite occurs around 4.5 Å, but the signal in this region is complex as there are multiple oxygen shells which occur at similar distances. The positions of these oxygen peaks are coherent with those previously presented for Sr:aragonite.[34,47] Aragonite $CaCO_3$ and strontianite $SrCO_3$ are isostructural (orthorhombic crystal system, *Pmcn* space group, Tab. S1). Sr–Ca distances in Sr:aragonite and Sr–Sr distances in strontianite are expected to be close, at 3.98(0)±0.03(6) Å and 4.15(5)±0.04(2) Å, respectively. Here, we additionally compared the imaginary parts of the FT between the reference strontianite and aragonite (Fig. 2, dotted lines). Indeed, the imaginary part of the EXAFS FT signal is expected to be more sensitive to a change in neighbouring element than the magnitude. The magnitude will reveal fine changes in radial distribution, while examination of the imaginary part permits a sensitive detection of phase shifts resulting from the exchange of the neighbouring atom Ca^{2+} for Sr^{2+} even associated to limited changes in interatomic distances. As shown in Fig. 2, the imaginary component of the FT for ancient otoliths is in very good agreement with that of the Sr:aragonite reference, while it is significantly different from strontianite.

We observed Sr as Sr:aragonite in all our archaeological and modern otolith specimens. A similar random substitution of Sr for Ca has been demonstrated in different species of corals, both modern[34,47,74–76] and ancient[74,76], the shell of a modern bivalve species[77], and statoliths or cuttlebones of two modern cephalopod species.[47] However, Greegor *et al.* identified strontianite domains within modern and ancient aragonitic corals[33] by fitting the FT magnitude of wide-beam EXAFS analyses with linear combinations of pure references (strontianite and Sr in aragonite). Our results therefore strongly support the presence of Sr in substitution for Ca in aragonite, rather than into all possible $CaCO_3$ mineral forms, in all ancient and modern samples studied. In total, four species from two families for a total of eight individuals and two different types of otoliths (sagittae and lapilli) were studied in the present work and Sr in an aragonitic environment was ubiquitously identified.

Focusing on modern samples, our results complement recent works that identified the random substitution of Sr^{2+} for Ca^{2+} in otoliths from ten modern individuals belonging to seven species from Australia using wide-beam EXAFS (*ca.* $0.3 \times 0.3 \text{ mm}^2$).[47] With the addition of our results, the random substitution of Sr^{2+} for Ca^{2+} in the otolith aragonite is now supported in a total of 6 teleost fish families for which either the sagittae or the lapilli are the most developed otoliths. The environments of the species

studied by Doubleday *et al.*[47] ranged from freshwater to hypersaline estuarine. Our corpus of samples brings an even broader diversity in fish ecology, as we have examined coastal marine species that can enter freshwater systems such as estuaries and lagoons.

4.2 Speciation in high Sr concentration features

The diversity in ecology of the fishes studied here and our methodology (quantification of Sr concentrations with μXRF coupled to XAS measurements) allowed a simultaneous extension of the conditions of Sr speciation to an increased range in Sr content. μXRF elemental mapping shows that the sections all have Sr distributed throughout their entirety with regular periodic variations in concentration along the growth axis, as expected for otoliths of individuals several years of age.[27,78]

Besides these periodic fluctuations, some individuals present one or several localized excursions from the mean Sr concentration that lay consistently along some of the growth increments. In HP-12 (Figs 1 and 5b) and HP -11 (Fig. 1), Sr excursions as high as $93.9\,\mu mol\cdot g^{-1}$ ($8230\,\mu g\cdot g^{-1}$) and $101\,\mu mol\cdot g^{-1}$ ($8848\,\mu g\cdot g^{-1}$) are measured, respectively. Growth features of high Sr concentrations may be located (a) in the bulk of the sample for QCD, BH17, 424 (shown in Cook *et al.*[27]), HP-11 (Fig. 1) and HP-12 (such as spots B, C, D, and E; Fig. 1), or (b) near the sample surface (where spot G was performed; Fig. 1; see next section) and at the edge for Bayovar-1C and 424 (shown in Cook *et al.*[27]).

Even in these cases at such elevated concentration, in all XANES spectra collected, all discriminating features universally pointed to Sr:aragonite (*Supplementary Information* Fig. S5). We therefore did not observe any change in Sr speciation in those internal high Sr concentration features, even though very high Sr contents — exceeding or equalling the maxima previously reported (up to $137\,\mu mol\cdot g^{-1}$)[79,80] — were measured in the archaeological *G. peruvianus* samples.

At the length scale of the increment thickness and at the limit in terms of attainable lateral resolution, an intriguing and yet unexplained behavior was observed. The fluctuation in Sr concentration appeared mostly anticorrelated to that in calcium. The Ca content of the otoliths was observed to vary up to 3.5 % of the median in the core to edge profiles produced by μXRF as exemplified for one archaeological and two modern individuals (Fig. 5). This is particularly noticeable for the most extreme Sr concentration features observed in the archaeological specimens QCD and HP-12 (Fig. 5a,b), and in the modern GP-292 (Fig. 5c). It is unlikely that this anticorrelation results from improper XRF matrix correction as the attenuation length of the Ca signal is altered by no more than 0.25 % across the range of Sr concentrations typically found in otoliths (0.05–0.5 %at). The variation in Ca is too large to be accounted for purely through increased substitution by Sr. Ca-depleted regions are likely to correspond to zones richer in organic matter. In our samples, even in those zones, Sr therefore appears to substitute randomly for Ca in an aragonitic chemical environment, with no evidence of Sr in another chemical environment. If confirmed, this anticorrelation may go unnoticed as the measured Sr concentration is usually normalised to Ca concentra-

(a) QCD

(b) HP-12
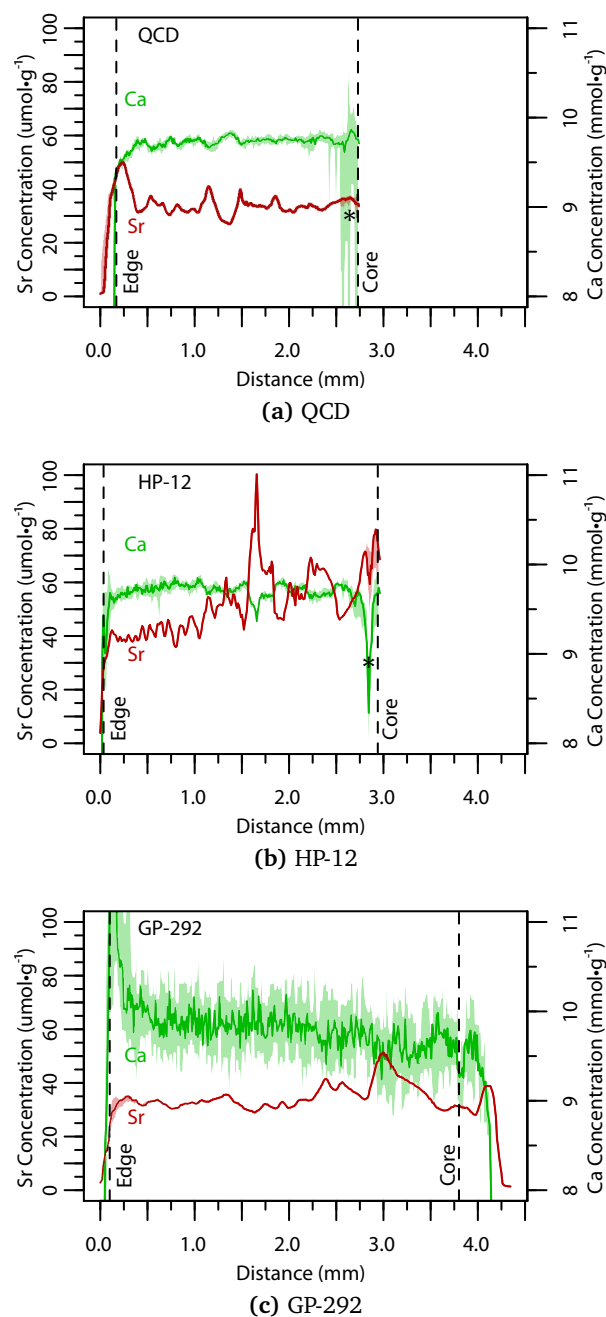
(c) GP-292

Fig. 5 Sr and Ca concentration profiles along the growth axis in archaeological samples from the Pacific coast of Peru: QCD (*Micropogonias* sp., Pampa de los fósiles, *n*=13, a) and HP-12 (*G. peruvianus*, Huaca Prieta, *n*=11, b), and modern reference sample GP-292 (*G. peruvianus*, *n*=11, c). Profiles were obtained by integrating bands of *n* pixels perpendicular to the growth axis on splines defined visually according to Sr fluctuations to conform to the otolith's curvature as previously described.[27] Asterisks mark the presence of physical cracks.

tion even where techniques yield absolute values (*e.g.* [49,81]), and deserves further investigation.

4.3 Extending determination of speciation to millimetric sample areas

Series of μXAS points can reveal Sr chemical environment at several distinct locations across a sample. However, the overall representativeness of microscale point analyses may be lower than that at millimetre scale because selection of the points could have, intentionally or not, avoided local singularities.

In order to validate the representativity of point analyses and trace potential high resolution spatial variations, a multi-energy μXANES mapping developed in this work examined a selected zone of $570 \times 450 \, \mu m^2$ of the archaeological sample QCD (Fig. 4). Mapping on the edge of the sample was chosen because, during burial, the outer surface of the otolith is expected to be the most vulnerable to alteration by being in direct contact with the decaying fish, as well as fluids and sediments from the environment. [28] The universal presence of Sr permitted microscale analysis at multiple points and at varying Sr concentrations. A map of Sr:aragonite fraction was calculated from the assumption that each XANES spectrum at Sr K-edge results from the linear combination of contributions from strontianite and aragonite domains.

The estimated aragonite fraction is largely homogeneous across the map (mean=91 %, SD=7.2 %; Fig. 4f). Importantly, we did not see any outlier hotspot of primarily strontianite on the whole map at a $6.0 \times 11 \, \mu m^2$ lateral resolution. The percentage of points outside of this 91 % is similar to the observed noise, attributed to the limited Sr XRF counts per pixel. A second calculation excluding the strontianite component (*i.e.* a pure aragonite system) was performed and achieved a mean adjusted r^2 of 0.992 for the overall map. Without completely ruling out the possible presence of strontianite domains as a (diluted) minor component of the probed information volumes due to the relatively high noise levels of the present measurement, a purely aragonite-type system where Sr would randomly substitute for Ca is therefore sufficient to explain the observed data. Based on simulated data derived from the reference spectra, it may be possible to detect the presence of as little as a 10 % strontianitic environment, *i.e.* 11 ng of strontianite per $6.0 \times 16 \, \mu m^2$ pixel. The presence of Sr–Sr neighbours resulting from random substitution has been suggested as a possible source for strontianite-type contributions to XAS spectra in aragonite regions of higher Sr concentration. [47] However, it appears relatively unlikely at our concentration. The expected probability to find Sr atoms with more than another Sr neighbour is very low – 1.6×10^{-3} % for the highest Sr concentration, observed on the sample border in the mapped zone. Contributions from random Sr–Sr pairs would therefore be negligible in our absorption spectra. The majority of points fell within the expected aragonite fraction range of 0 to 1, although no corresponding constraint was applied to the model. Several outlier points (*ca.* 1.4 SD from the mean) occurred above 1.0, to a maximum of 1.18. This further supports the model's accuracy by demonstrating that, even without constraining the fraction to the expected interval, the majority of values fall within a reasonable range.

Fast μXANES mapping at high resolution over a large area offers for the first time the ability to study Sr speciation over 'large spatial dynamics'[48] covering 2 orders of magnitude from *ca.* 10 μm to the millimetre range, in order to identify heterogeneity at any length scale. For all analyses, an effort was made to maximise lateral resolution along the growth axis (see Fig. 4a). Annual growth increments in fish otoliths are perpendicularly oriented relative to the growth axis and were observed to be 70–140 μm in width in QCD.[27] As a result, the QCD maps crossed two sequential isochronous increments, and allowed measurements at high resolution within a single increment. The information volume for this analysis is identical to that previously described for point μXAS and is on the same order of size as the needle-like crystalline units composing individual increments which are visible on etched sections under SEM (see Fig. 2 in Dauphin *et al.* [8]).

μXRF mapping at the edge of the QCD sample showed that the analysed zone exhibits significant variation in Sr content, including the largest variation for the whole specimen. Increased Sr concentration near to the surface could alternatively be interpreted as a specific event at the end of the life of the specimen as a similar feature was observed in a modern *Micropogonias* sp. specimen (424), or as resulting from *post-mortem* Sr deposition. μXRF mapping of Fe, Cu and Zn revealed an increase of these elements no deeper than a few hundred micrometres in QCD. These elements could be used as secondary markers of the uptake of exogenous elements. A near to the edge increase of these elements was however also observed in 424 that was not in contact with a burial environment. [27] It was therefore not possible to conclude on the biogenic or *post-mortem* origin of the Sr localized excursion in QCD. As our mapping approach demonstrates that no other Sr speciation than the Sr:aragonite observed in the bulk of the sample is present within the limits of detection close to the sample surface, any possible Sr incorporated *post-mortem* must have been integrated into an aragonitic environment. Caution is therefore advised as exogenous Sr coming from the environment might be incorporated in the same aragonitic environment as the pristine signal from the life of the fish. However, as a markedly monotonous decrease in Sr concentration is observed from the surface to a depth of a few hundred micrometres[27], exogenous Sr uptake, should it be the case, does not appear to extend further into the bulk.

5 Conclusion

Ancient otoliths are increasingly used as environmental proxies for palaeoenvironmental reconstructions and archaeological studies, yet very little is known on the chemistry of their alteration and possible changes to the chemically-encoded information. The Peruvian otoliths studied here are likely to have experienced limited exposure to fluids after their initial taphonomy, due to the exceptional climatic conditions that prevail on the Pacific coast. Coastal fogs that form during the austral winter are the main source of humidity in the very arid environment while intense precipitation is mostly limited to El Niño events. Moreover, the otoliths in the present work originate from two sandy surface sites (Bayovar-1 and Pampa de los fósiles) deprived of pore water and from one stratified mound (Huaca Prieta) not susceptible

to significant ground water exposure. Prevailing climatic conditions on the Peruvian and Chilean coasts have favored the conservation of Holocene bivalve or gastropod shells[25,82], limiting the diagenetic alteration, or on the contrary led to their rapid diagenesis, thereby precluding palaeoenvironmental reconstructions based on geochemical analyses.[83] In the latter case, the shells originated from emerged marine terraces. Macroscopic examination showed that the aragonitic layer was frequently pulverulent. Early diagenesis during marine immersion is evidenced by a marine uranium/thorium signal. Later contamination by sea spray could be present as an agent of alteration, but the effects are expected to be very limited compared to immersion.[83] Samples from marine sites may undergo significant alteration as a result of the circulation of pore water in the surrounding sediment. Even in the case of otoliths recovered from favourable deposition environments, actions by the ancient humans who consumed the fish could produce alteration. Cooking and burning, for example, have been shown to alter the mineralogy and elemental concentrations in otoliths.[71] The minor and trace elements in otoliths are often difficult to analyse due to their low concentrations. In cases where there is no apparent structural alteration, the impact of infiltrated or leached elements on the overall sample may go unnoticed, making a targeted analysis of the potentially-altered element necessary.

This work presents the first examination of the chemical environment of strontium in archaeological otoliths. Five archaeological and three modern otoliths of fish from two families (Sciaenidae and Ariidae) were examined using a newly developed multiscale synchrotron-based approach. Elemental mapping by synchrotron µXRF permitted a precise positioning of analyses on the otolith sections in relation to the sub-annual fluctuations of Sr. XAS is the optimal choice for targeted analyses of ion incorporation and speciation in heterogenous systems.[84] The chemical environment of Sr^{2+} in a set of archaeological and modern fish otoliths has been examined on the microscale using µEXAFS and µXANES. µEXAFS proved very efficient to discriminate Sr:aragonite against other possible mineral forms owing to the contrast in phase shift between Ca and Sr. Multi-energy µXANES mapping was developed to study the speciation homogeneity over a $480 \times 550 \mu m^2$ area in a reasonable time frame. Sr^{2+} was confirmed in all cases to substitute randomly for Ca^{2+} in the aragonite lattice, independent of location on the otolith, Sr concentration — even in the case of extremely high content noted along specific growth increments, or archaeological age of the otolith. Some samples may contain exogenous Sr in the first few hundreds of micrometers from their surface. If the extra Sr is of exogenous origin, as no change in Sr speciation was observed, caution is advised as Sr could actually incorporate in the same aragonitic environment as the pristine palaeo-environmental signal with no known way to discriminate one from the other. Apart from this word of caution, this work further supports the validity of fish otoliths as an invaluable biological and palaeoenvironmental archive, as no microscale change of speciation is observed across the bulk of archaeological otoliths over time that could bias collection of the palaeo-environmental signal. The combination of synchrotron-based X-ray spectroscopies demon-

strated in the present work is shown to be a powerful and efficient method for the examination of biominerals and elucidation of incorporation mechanisms of trace elements.

References

1 D. Nolf, *Otolithi Piscium*, Gustav Fischer Verlag, Stuttgart, Germany, 1985.

2 E. Degens, W. Deuser and R. Haedrich, *Marine Biology*, 1969, **2**, 105–113.

3 D. Carlström, *Biological Bulletin*, 1963, **125**, 441–463.

4 R. Gauldie, *Journal of Morphology*, 1993, **218**, 1–28.

5 M. Strong, J. Neilson and J. Hunt, *Canadian Journal of Fisheries and Aquatic Sciences*, 1986, **43**, 1457–1463.

6 J. Tomas and A. Geffen, *Journal of Fish Biology*, 2003, **63**, 1383–1401.

7 P. Béarez, G. Carlier, J. Lorand and G. Parodi, *Comptes Rendus Biologies*, 2005, **328**, 243–252.

8 Y. Dauphin and E. Dufour, *Micron*, 2008, **39**, 891–896.

9 D. Jacob, A. Soldati, R. Wirth, J. Huth, U. Wehrmeister and W. Hofmeister, *Geochimica et Cosmochimica Acta*, 2008, **72**, 5401 – 5415.

10 S. Campana, *Marine Ecology Progress Series*, 1999, **188**, 263–297.

11 C. Q. Albuquerque, N. Miekeley, J. H. Muelbert, B. D. Walther and A. J. Jaureguizar, *Marine Biology*, 2012, **159**, 2229–2239.

12 T. Elsdon and B. Gillanders, *Reviews in Fish Biology and Fisheries*, 2003, **13**, 217–235.

13 T. Elsdon and B. Gillanders, *Journal of Experimental Marine Biology and Ecology*, 2004, **313**, 269–284.

14 T. Elsdon and B. Gillanders, *Marine Ecology Progress Series*, 2005, **285**, 233–243.

15 S. Campana, *Marine and Freshwater Research*, 2005, **56**, 485–495.

16 S. Carpenter, J. Erickson and F. Holland, *Nature*, 2003, **423**, 70–74.

17 C. Wurster and W. Patterson, *Paleobiology*, 2003, **29**, 492–505.

18 W. P. Patterson, *Palaeogeography, Palaeoclimatology, Palaeoecology*, 1998, **138**, 271 – 303.

19 M. Aubert, I. S. Williams, K. Boljkovac, I. Moffat, M.-H. Moncel, E. Dufour and R. Grün, *Journal of Archaeological Science*, 2012, **39**, 3184 – 3194.

20 D. Vanhove, P. Stassen, R. P. Speijer, P. Claeys and E. Steurbaut, *Austrian Journal of Earth Sciences*, 2012, **105**, 200–207.

21 M. Disspain, L. A. Wallis and B. M. Gillanders, *Journal of Archaeological Science*, 2011, **38**, 1842–1857.

22 K. Long, N. Stern, I. S. Williams, L. Kinsley, R. Wood, K. Sporcic, T. Smith, S. Fallon, H. Kokkonen, I. Moffat and R. Grün, *Quaternary Science Reviews*, 2014, **88**, 82–95.

23 A. K. Hufthammer, H. Høie, A. Folkvord, A. J. Geffen, C. Andersson and U. S. Ninnemann, *Journal of Archaeological Science*, 2010, **37**, 78–83.

24 M. C. F. Disspain, C. J. Wilson and B. M. Gillanders, *Archaeology in Oceania*, 2012, **47**, 141–150.

25 M. Carré and E. Dufour, in *Prehistoria de la costa extremo-sur del Perú: los pescadores arcaicos de la Quebrada de los Burros (10000–7000 a. P.)*, ed. D. Lavallée and M. Julien, Instituto Francés de Estudios Andinos, 2012, ch. 5, pp. 195–202.

26 E. Dufour, H. Cappetta, A. Denis, Y. Dauphin and A. Mariotti, *Bulletin de la Société géologique de France*, 2000, **171**, 521–532.

27 P. K. Cook, M.-A. Languille, É. Dufour, C. Mocuta, O. Tombret, F. Fortuna and L. Bertrand, *Chem. Geol.*, 2015, **414**, 1–15.

28 C. N. Trueman, *Palaeontology*, 2013, **56**, 475–486.

29 R. Gauldie and G. Coote, *Fisheries Science*, 1997, **63**, 486–487.

30 R. Parkman, J. Charnock, F. Livens and D. Vaughan, *Geochimica et Cosmochimica Acta*, 1998, **62**, 1481–1492.

31 P. O'Day, M. Newville, P. Neuhoff, N. Sahai and S. Carroll, *Journal of Colloid and Interface Science*, 2000, **222**, 184–197.

32 D. M. Singer, S. B. Johnson, J. G. Catalano, F. Farges and G. E. Brown, Jr., *Geochimica et Cosmochimica Acta*, 2008, **72**, 5055–5069.

33 R. Greegor, N. Pingitore and F. Lytle, *Science*, 1997, **275**, 1452–1454.

34 A. Finch, N. Allison, S. Sutton and M. Newville, *Geochimica et Cosmochimica Acta*, 2003, **67**, 1197–1202.

35 P. Béarez, E. Dufour, J. Crédou and C. Chauchat, in *Peuplements et préhistoire en Amériques*, ed. D. Vialou, CTHS, 2011, pp. 233–246.

36 T. D. Dillehay, D. Bonavia, S. Goodbred, M. Pino, V. Vasquez, T. Rosales Tham, W. Conklin, J. Splitstoser, D. Piperno, J. Iriarte, A. Grobman, G. Levi-Lazzaris, D. Moreira, M. Lopéz, T. Tung, A. Titelbaum, J. Verano, J. Adovasio, L. S. Cummings, P. Béarez, E. Dufour, O. Tombret, M. Ramirez, R. Beavins, L. DeSantis, I. Rey, P. Mink, G. Maggard and T. Franco, *Antiquity*, 2012, **86**, 48–70.

37 N. Goepfert, P. Béarez, A. Christol, B. Gutiérrez and P. Wuscher, *The fishermen of Sechura: excavations at a specialised site from the Early Intermediate Period, extreme northern Peru*, 2014, http://journal.antiquity.ac.uk/projgall/goepfert340.

38 C. Chauchat and J. Pélegrin, *Bulletin de la Société préhistorique française*, 1994, **91**, 275–280.

39 D. Nolf, *The Diversity of fish otoliths, past and present*, Royal Belgian Institute of Natural Sciences, Brussels, Belgium, 2013.

40 J. Yoshinaga, A. Nakama, M. Morita and J. Edmonds, *Marine Chemistry*, 2000, **69**, 91–97.

41 SOLEIL synchrotron, Gif-sur-Yvette, France, *Diffabs beamline*, http://www.synchrotron-soleil.fr/Recherche/LignesLumiere/DIFFABS.

42 P. Kirkpatrick and A. V. Baez, *J. Opt. Soc. Am.*, 1948, **38**, 766–774.

43 V. Solé, E. Papillon, M. Cotte, P. Walter and J. Susini, *Spectrochimica Acta Part B: Atomic Spectroscopy*, 2007, **62**, 63–68.

44 B. Ravel and M. Newville, *Journal of Synchrotron Radiation*, 2005, **12**, 537–541.

45 P. Gueriau, C. Mocuta and L. Bertrand, *Anal. Chem.*, 2015, **87**, 8827–8836.

46 R Core Team, *R: A Language and Environment for Statistical Computing*, R Foundation for Statistical Computing, Vienna, Austria, 2014.

47 Z. A. Doubleday, H. H. Harris, C. Izzo and B. M. Gillanders, *Analytical Chemistry*, 2014, **86**, 865–869.

48 L. Bertrand, M. Thoury and E. Anheim, *Journal of Cultural Heritage*, 2013, **14**, 277–289.

49 K. E. Limburg, C. Olson, Y. Walther, D. Dale, C. P. Slomp and H. Høie, *Proceedings of the National Academy of Sciences of the United States of America*, 2011, **108**, E177–E182.

50 M. Carré and E. Dufour, in *Prehistoria de la costa extremo-sur del Perú: los pescadores arcaicos de la Quebrada de los Burros (10000–7000 a. P.)*, ed. D. Lavallée and M. Julien, Instituto Francés de Estudios Andinos, 2012, ch. 5, pp. 195–202.

51 B. K. Nelson, M. J. Deniro, M. J. Schoeninger, D. J. D. Paolo and P. Hare, *Geochimica et Cosmochimica Acta*, 1986, **50**, 1941–1949.

52 R. E. M. Hedges, *Archaeometry*, 2002, **44**, 319–328.

53 M. J. Collins, C. M. Nielsen-Marsh, J. Hiller, C. I. Smith, J. P. Roberts, R. V. Prigodich, T. J. Wess, J. Csapò, A. R. Millard and G. Turner-Walker, *Archaeometry*, 2002, **44**, 383–394.

54 M. Lebon, K. Müller, J.-J. Bahain, F. Fröhlich, C. Falguères, L. Bertrand, C. Sandt and I. Reiche, *J. Anal. At. Spectrom.*, 2011, **26**, 922–929.

55 K. A. Hoppe, P. L. Koch and T. T. Furutani, *International Journal of Osteoarchaeology*, 2003, **13**, 20–28.

56 E. A. Hinz and M. J. Kohn, *Geochimica et Cosmochimica Acta*, 2010, **74**, 3213–3231.

57 J. Chappell and H. A. Polach, *Quaternary Research*, 1972, **2**, 244–252.

58 B. Buchardt and S. Weiner, *Sedimentology*, 1981, **28**, 423–438.

59 L. Cherns, J. Wheeley and V. Wright, in *Taphonomy*, ed. P. A. Allison and D. J. Bottjer, Springer Netherlands, 2011, vol. 32, pp. 79–105.

60 N. P. James, *Journal of Paleontology*, 1974, **48**, 785–799.

61 G. E. Webb, L. D. Nothdurft, B. S. Kamber, J. T. Kloprogge and J.-X. Zhao, *Sedimentology*, 2009, **56**, 1433–1463.

62 Z. Kern, M. Kázmér, M. Bosnakoff, T. Váczi, B. Bajnóczi and L. Katona, *Geologica Carpathica*, 2012, **63**, 175–178.

63 D. Vanhove, P. Stassen, R. P. Speijer and E. Steurbaut, *Geologica Belgica*, 2011, **14**, 143–158.

64 C. Wurster and W. Patterson, *Palaeogeography, Palaeoclimatology, Palaeoecology*, 2001, **170**, 81–100.

65 A. J. Geffen, H. Høie, A. Folkvord, A. K. Hufthammer, C. Andersson, U. Ninnemann, R. B. Pedersen and K. Nedreaas, *ICES Journal of Marine Science*, 2011, **68**, 1081–1089.

66 J. A. Speer, in *Carbonates: Mineralogy and Chemistry*, ed. R. J. Reeder, Mineralogical Society of America, Washington, DC, 1983, vol. Volume 11: Carbonates, ch. 5, pp. 145–190.

67 R. D. Shannon, *Acta Crystallographica Section A*, 1976, **32**, 751–767.

68 J. De Villiers, *American Mineralogist*, 1971, **56**, 758–767.

69 R. Gauldie, C. Thacker, I. West and L. Wang, *Comparative Biochemistry and Physiology – Part A: Molecular & Integrative Physiology*, 1998, **120**, 551–556.

70 D. Milton and S. Chenery, *Journal of Fish Biology*, 1998, **53**, 785–794.

71 C. Andrus and D. Crowe, *Journal of Archaeological Science*, 2002, **29**, 291–299.

72 C. H. Proctor and R. E. Thresher, *Marine Biology*, 1998, **131**, 681–694.

73 A. A. Finch and N. Allison, *Mineralogical Magazine*, 2007, **71**, 539–552.

74 A. Finch and N. Allison, *Geochimica et Cosmochimica Acta*, 2003, **67**, 4519–4527.

75 N. Allison, A. Finch, M. Newville and S. Sutton, *Geochimica et Cosmochimica Acta*, 2005, **69**, 3801–3811.

76 N. Allison, A. Finch, S. Sutton and M. Newville, *Geochimica et Cosmochimica Acta*, 2001, **65**, 2669–2676.

77 L. C. Foster, N. Allison, A. A. Finch and C. Andersson, *Geochemistry Geophysics Geosystems*, 2009, **10**, 1–14.

78 J. Kalish, *Journal of Experimental Marine Biology and Ecology*, 1989, **132**, 151–178.

79 A. R. Munro, T. E. McMahon and J. R. Ruzycki, *Canadian Journal of Fisheries and Aquatic Sciences*, 2005, **62**, 79–87.

80 Y.-J. Lin, B. M. Jessop, O. L. Weyl, Y. Iizuka, S.-H. Lin and W.-N. Tzeng, *Environmental Biology of Fishes*, 2015, **98**, 457–468.

81 K. E. Limburg, B. D. Walther, Z. Lu, G. Jackman, J. Mohan, Y. Walther, A. Nissling, P. K. Weber and A. K. Schmitt, *Journal of Marine Systems*, 2015, **141**, 167–178.

82 N. Guzmán, Y. Dauphin, J. P. Cuif, A. Denis and L. Ortlieb, *Biogeosciences*, 2009, **6**, 197–207.

83 M. Labonne and C. Hillaire-Marcel, *Geochimica et Cosmochimica Acta*, 2000, **64**, 1523–1534.

84 L. Bertrand, M. Cotte, M. Stampanoni, M. Thoury, F. Marone and S. Schöder, *Phys. Rep.*, 2012, **519**, 51–96.

85 L. Bertrand, M.-A. Languille, S. X. Cohen, L. Robinet, C. Gervais, S. Leroy, D. Bernard, E. Le Pennec, W. Josse, J. Doucet and S. Schöder, *Journal of Synchrotron Radiation*, 2011, **18**, 765–772.

86 E. Caspi, B. Pokroy, P. Lee, J. Quintana and E. Zolotoyabko, *Acta Crystallographica Section B-Structural Science*, 2005, **61**, 129–132.

87 H. Swanson and R. Fuyat, *Circular of the Bureau of Standards: Standard X-ray diffraction powder patterns*, National Bureau of Standards, 1953.

88 S. R. Kamhi, *Acta Crystallographica*, 1963, **16**, 770–772.

89 R. L. Sass, R. Vidale and J. Donohue, *Acta Crystallographica*, 1957, **10**, 567–570.

90 S. Hayakawa, Y. Hajima, S. Qiao, H. Namatame and T. Hirokawa, *Analytical Sciences*, 2008, **24**, 835–837.